ACSNANO

www.acsnano.org

ARTICLE

Self-illuminating NIR-II bioluminescence imaging probe based on silver sulfide quantum dots

Mohammad Javad Afshari, Cang Li, Jianfeng Zeng, Jiabin Cui, Shuwang Wu, and Mingyuan Gao*

Cite This: *ACS Nano* 2022, 16, 16824–16832

Read Online

ACCESS | Metrics & More | Article Recommendations | Supporting Information

ABSTRACT: **Bioluminescence (BL) imaging has emerged to tackle the potential challenges of fluorescence (FL) imaging including the autofluorescence background, inhomogeneous illumination over a wide imaging field, and the light-induced overheating effect. Taking advantage of the bioluminescence resonance energy transfer (BRET) mechanism between a conventional luciferin compound and a suitable acceptor, the visible light of the former can be extended to photons with longer wavelengths emitting from the latter. Although BRET-based self-illuminating imaging probes have already been prepared, employing potentially cytotoxic elements as the acceptor with the emission wavelengths which hardly reach the first near-infrared (NIR-I) window, has limited their applications as safe and high performance *in vivo* imaging agents. Herein, we report a biocompatible, self-illuminating, and second near-infrared (NIR-II) emissive probe to address the cytotoxicity concerns as well as improve the penetration depth and spatiotemporal resolution of BL imaging. To this end, NanoLuc luciferase enzyme molecules were immobilized on the surface of silver sulfide quantum dots to oxidize its luciferin substrate and initiate a single-step BRET mechanism, resulting in NIR-II photons from the quantum dots. The resulting dual modality (BL/FL) probes were successfully applied to *in vivo* tumor imaging in mice, demonstrating that NIR-II BL signals could be easily detected from the tumor sites, giving rise to ~2 times higher signal-to-noise ratios compared to those obtained under FL mode. The results indicated that nontoxic NIR-II emitting nanocrystals deserve more attention to be tailored to fill the growing demands of preparing appropriate agents for high quality BL imaging.**

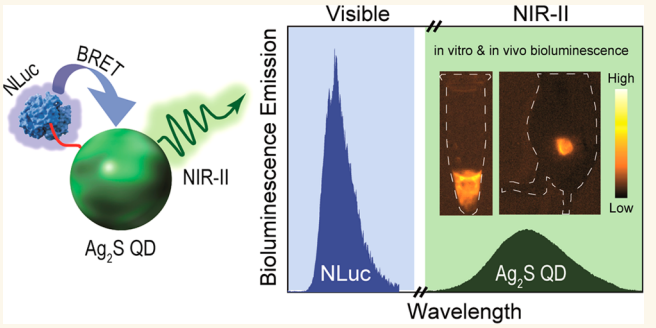

KEYWORDS: *Bioluminescence imaging, Bioluminescence resonance energy transfer, Silver sulfide, Quantum dots, NanoLuc luciferase*

INTRODUCTION

Fluorescence imaging is one of the well-known cancer detection techniques, taking advantage of favorable characteristics such as being noninvasive, real-time, free of ionizing radiation, and highly sensitive.[1] In general, fluorescence imaging requires an energy input to excite the fluorescent probe as well as an appropriate detector to collect and process the fluorescence signals. However, the excitation light can induce a series of unfavorable effects, *e.g.*, water- and/or hemoglobin-mediated photon to heat conversion, inhomogeneous light illumination over the area of interest, *etc.*, which may lead to signal intensity distortion, impairing the imaging resolution in long-time *in vivo* imaging.[2−5] To address these issues, excitation-free techniques such as chemiluminescence, afterglow and bioluminescence imaging, in which the excitation source has been replaced by an internal energy donor, are gaining growing attractions.[6,7] However, these self-illuminating modalities are still in their infancy, leaving ample room for further improvements. For instance, most of the current chemiluminescent systems face the issue of unsatisfactory quantum yield (QY) and the majority of afterglow imaging agents suffer from nonideal lifetime and low brightness. Moreover, poor biocompatibility and low imaging penetration depth are common features of most of the excitation-free imaging agents, especially bioluminescent probes.[6]

The low penetration depth of bioluminescence probes is attributed to the emission mechanism. Bioluminescence

Received: July 6, 2022
Accepted: September 28, 2022
Published: September 30, 2022

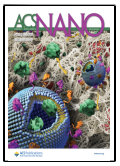

imaging is based on the phenomenon which occurs naturally in some living creatures such as marine organisms, fungi, insects, *etc.*, as a part of their biological behaviors.[8] The process involves a catalytic redox reaction between a light emitting compound (luciferin) and a suitable enzyme (luciferase) as the catalyst. However, the resulting light falls in the visible range, resulting in low penetration depth. Therefore, numerous attempts have been made to extend the emission to longer wavelengths to improve the penetration performance. As one of the approaches to accomplish this goal, utilizing acceptors for transferring the high energy released by the emission systems (as the donor) to generate red-shifted signals through a single or multiple bioluminescence/fluorescence resonance energy transfer (BRER/FRET) mechanisms can be mentioned. Alternatively, some researchers have attempted to structurally alter luciferins or luciferases in order to provide red-shifted photons pushing bioluminescence imaging to the first near-infrared window (NIR-I, *ca.*, 650−950 nm). Meanwhile, due to the minimized photon scattering and almost faded background from the tissue autofluorescence, it is strongly desired to synthesize bioluminescent probes with the emission in the second near-infrared window (NIR-II, *ca.*, 1000−1700 nm) to further increase the penetration depth and spatiotemporal resolution. Following the discovery, nanoparticles emitting lights in the NIR-II window have attracted considerable attention in the field of bioimaging during the past decade.[9−12]

A pioneering study performed by Rao's group utilized quantum dots (QDs) as the acceptor of BRET mechanism, taking advantage of their high QY, photostability, relatively straightforward synthesis protocols, and large molar extinction coefficients.[13] Thus far, many QD-based bioluminescent probes have been reported for quantifying the enzymatic activity,[14,15] nucleic acid detection,[16,17] cellular protein interaction,[18] insemination investigation,[19] photodynamic therapy,[20] *in vivo* cell tracking,[21] and tumor or lymph node imaging.[22−28] However, the studies mentioned above have the imperfection of utilizing dyes or cadmium-based QDs, which are notorious for either photobleaching or cytotoxicity or both, hindering the clinical applications. Besides, neither of the aforementioned probes could establish their detection territories to the NIR-II region, resulting in severely distorted signal detection from deep tissues. Until now, there are only a few non-QD-based reports of successfully developed bioluminescent probes with NIR-II emission. As an example, a NIR-II dye (FD-1029) based bioluminescent probe has been recently developed by taking advantage of a sequential BRET-FRET-FRET energy transfer between D-luciferin substrate and three different dyes, namely, Cy7.5, Cy5, and FD-1029. Nevertheless, utilizing several dyes as the main constituents of the probe might render the design and synthesis processes intricate, since robust optimizations need to be performed to obtain the optimal ratio among the molecules in order to avoid the self-quenching effect. Moreover, the relay of energy transferring steps might inevitably lead to the loss of energy, decreasing the total efficiency of the transferring.[2] These pioneering studies encouraged us to research bioluminescent probes with the emission of NIR-II which would realize imaging deep tissues with high sensitivity, biocompatibility, and photostability, pushing bioluminescent probes forward to clinical applications. Developing NIR-II emissive sliver sulfide (Ag_2S) QDs by Wang *et al.* has been considered one of the most important advances in synthesizing NIR-II emitting materials, offering promising probes for real-time and deep-tissue noninvasive *in vivo* imaging.[29−38] Their biocompatibility, which might be attributed to their ultralow solubility product constant ($K_{sp} = 6.3 \times 10^{-50}$),[38] as well as long wavelength emitting capability, make Ag_2S QD an interesting candidate to serve as the acceptor in a BRET system to develop self-illuminating bioluminescence probes with the capability of emitting in NIR-II window.

Herein, we employed Ag_2S QDs as a NIR-II emitter acceptor for bioluminescence imaging, to overcome the cytotoxicity problem of the conventional QD-based bioluminescent probes and also improve the imaging penetration depth and resolution. With this aim in mind, first, the efficacy of the prepared Ag_2S QDs as an *in vivo* imaging agent was confirmed by exploiting its fluorescence emission under 808 nm laser excitation. Following the confirmation, luciferase enzyme molecules were anchored to the surface of the QDs to prepare a self-illuminating probe. In the presence of luciferin substrate, the BRET mechanism can be initiated by transferring redox-mediated energy to Ag_2S QDs, inducing them to illuminate NIR-II photons. To ensure a high degree of spectral overlap between the donor and acceptor as well as provide a glow-type luminescence, NanoLuc luciferase (NLuc) together with its substrate, furimazine, was utilized in this study. Unlike some luciferase−luciferin reactions, the oxidizing reaction between these reactants only requires oxygen molecules as the cofactor. Moreover, in comparison with other popular luciferases such as firefly and *Renilla*, NLuc offers some distinct advantages including smaller size and enhanced pH and temperature stability which are favorable properties for engaging in *in vivo* imaging applications.[8,39]

RESULTS

Preparation and Basic Characterization of the Probes. Hydrophobic silver sulfide QDs were synthesized following a previously reported protocol,[29] with some minor modifications. The native alkyl-thiol ligands of the as-prepared samples were exchanged with 11-mercaptoundecanoic acid (MUA) and the resulting hydrophilic products (QD-MUA) underwent two different synthesis routes to construct fluorescent (FL) and bioluminescent (BL) probes. The routes are comprehensively described in the Supporting Information (Figures S1 and S2) and briefly illustrated in Figure 1a. In order to delay the elimination of the probe from blood circulation,[40] 6-arm amine functionalized PEG were utilized to wrap the QDs, forming FLQDs and BLQDs. Furthermore, owing to their strong affinity toward $\alpha_v\beta_3$ receptors which are overexpressed on the surface of many malignant tumors,[41] cRGD peptides were anchored to the surface of the resulting conjugates to facilitate the active tumor targeting toward murine 4T1 breast cancer tumor model, providing c-FLQDs and c-BLQDs. FL samples were mainly employed to investigate the proper *in vivo* performance of the as-prepared probes, while BL ones were employed to explore self-illuminating properties.

The TEM study resulted in mean size of 5.5 ± 0.6 and 5.7 ± 0.7 nm for hydrophobic mother particles and the hydrophilic BLQDs samples, respectively (Figure S3 and Figure 1b). The mean hydrodynamic sizes of the samples were measured by dynamic light scattering (DLS) and determined to be 8.7, 15.7, and 18.2 nm for QD-MUA, c-FLQDs, and c-BLQDs, respectively (Figure 1c). The results of TEM and DLS analyses indicated that the prepared probes have favorable sizes and monodispersity for taking part in *in vivo*

https://doi.org/10.1021/acsnano.2c06667
ACS Nano 2022, 16, 16824−16832

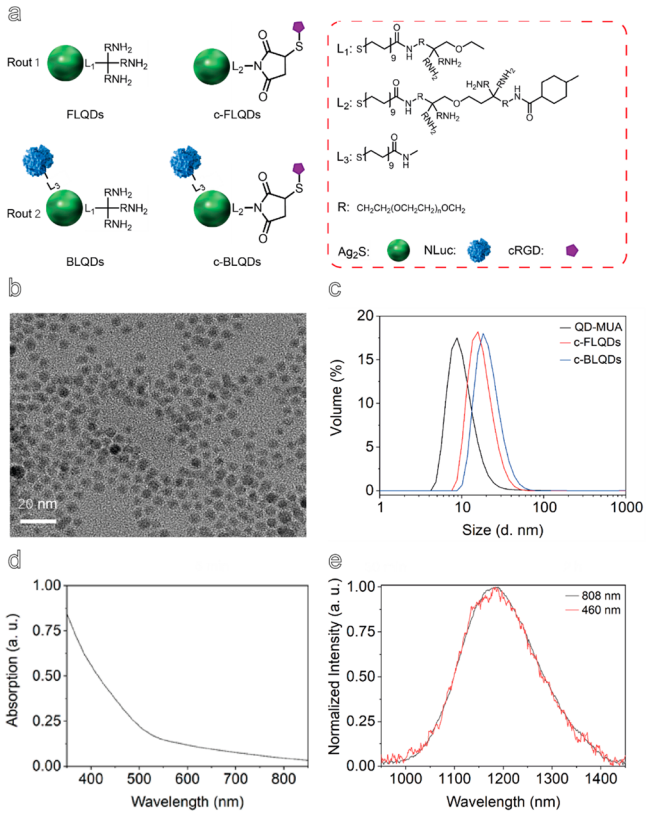

Figure 1. (a) Schematic illustration of the surface coating of the as-prepared probes via routes 1 and 2. (b) TEM image of hydrophilic BLQDs probe. (c) Hydrodynamic size distribution of the as-prepared hydrophilic samples. Absorption (d) and emission spectra (e) of the as-synthesized QDs. The emission spectra were collected either under 808 nm laser or 460 nm xenon lamp excitation.

applications.[40] Following the surface modification steps, first, the negatively charged carboxyl groups of the QD-MUA probe would get passivated by forming carbodiimide bonds with positively charged amine groups of PEG. Then, NLuc which has the isoelectric point of 5 and a negative surface charge in neutral pH would be introduced to the decoration through the same binding strategy. As a consequence, the surface charge of the QD-MUA probe was decreased from −41.9 ± 2.1 to +1 ± 0.1 and −4.8 ± 0.3 mV, for c-FLQDs and c-BLQDs, respectively (Figure S4a). Since samples with different sizes would experience different mobilities following the passage through the gel matrix, agarose gel electrophoresis was performed to verify the successful conjugation steps. The lane loaded with c-BLQDs, as shown in Figure S4b, encountered lower mobility compared to those loaded with c-FLQDs and QD-MUA, respectively, indicating the size enhancement following the occurrence of enzyme and PEG conjugation. Bradford protein assay was utilized to estimate the approximate number of NLuc molecules on the surface of a single QD. The result led to an assumption that ∼10 enzyme molecules were loaded on the surface of each QD (Figure S5). Even though the higher enzyme loading number might be favorable to increase BRET signal intensity,[13] increasing the parameter would presumably lead to a higher steric hindrance as well as fewer available ligands for the PEGylation step. Furthermore, in order to investigate the colloidal stability of the probes, BLQDs and FLQDs were stored in Tris buffer as well as DMEM culture medium supplemented with 10% FBS and 0.9% NaCl, up to 48 h at 4 °C. The lack of significant difference in hydrodynamic sizes of the probes during the storage period suggested their high colloidal stability (Figure S6a and b). In addition, no precipitation or aggregation was observed during one month of storing BLQDs in Tris buffer at room temperature. However, storing the probe at room temperature would lead to a drastic decrease in enzyme activity (Figure S7). Additionally, the probes exhibited a broad and featureless absorbance spectrum, illustrated in Figure 1d, covering a wide range of wavelengths, from the NIR to the visible region. The spectrum revealed that the prepared QDs might be capable of strongly absorbing the visible light emitting from different kinds of luciferins. It is worth noting that the lack of a discrete absorbance band, which distinguishes the absorption spectra of Ag_2S QDs from those of most of the II−VI QDs, originates in the difference between the electronic properties of these two classes of nanocrystals.[42,43] Moreover, as shown in Figure 1e, following the excitation under either 808 nm light provided by laser or 460 nm photons arising from the xenon lamp, emission profiles in the NIR-II region from 1000 to 1400 nm with a peak at ∼1200 nm and ∼195 nm full width at half-maximum (FWHM) were obtained. The fluorescence intensity of the FLQDs showed negligible variation during 48 h of incubation in DMEM culture medium supplemented with 10% FBS and 0.9% NaCl (Figure S6c), demonstrating their fluorescence stability.

In Vitro Performance of the Probes. The *in vitro* cytotoxicity of the probes was assessed by incubating different concentrations of FLQDs and c-FLQDs probes with 4T1 breast cancer cell line, for 48 h. The cell viability values given in Figure 2a suggested that the probes with concentration as high as 100 μg/mL did not induce any noticeable cell death, demonstrating their excellent biocompatibility with 4T1 cells. It is worth mentioning that the highest concentration in this experiment (100 μg/mL) was chosen as such to be well above the level expected to accumulate in tumor and major organs, following intravenous injection of Ag_2S based probes.[29,35]

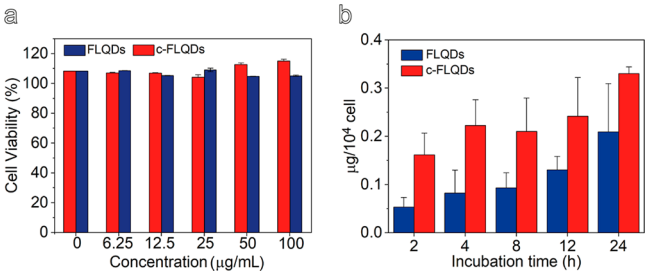

Figure 2. (a) Viability percentages of 4T1 cells incubated with different concentrations of probes for 48 h. (b) Amount of QDs uptaken by 4T1 cells at different incubation time intervals. The error bars represent the standard deviation (n = 6).

Furthermore, the *in vitro* cell targeting ability of the samples was evaluated by incubating the cRGD- and non-cRGD-conjugated probes with 4T1 cells for different time intervals. Subsequently, the amount of QDs internalized inside the cells was measured. As seen from Figure 2b, at each specific time point, the cells incubated with c-FLQDs probes exhibited higher silver uptake compared to the FLQDs group, verifying the superior *in vitro* cell targeting ability of the cRGD-conjugated probes. Owing to the strong affinity of cRGD

https://doi.org/10.1021/acsnano.2c06667
ACS Nano 2022, 16, 16824−16832

peptides toward $\alpha_v\beta_3$ receptors which are overexpressed on 4T1 cells, the internalization mechanism of c-FLQDs is expected to be via integrin-mediated endocytosis.[41] On the other hand, with respect to the size and surface charge of FLQDs probe, clathrin mediated endocytosis (CME) might presumably be their dominant internalization pathway.[44] Although prolonging the incubation time up to 24 h led to an increase in the silver uptake for both groups, further extending the period did not lead to a significant increase in the nanoparticle internalization. In general, the bigger size of QDs compared to small molecule based nanoprobes hinders them from freely perfusing on the membrane in order to access the bottom contact area of the adherent cells.[29] As a consequence, fewer receptors might be available for QDs to bind, preventing them from exhibiting significantly higher cell accumulation values for longer incubation times.

In Vivo Performance of the Probes. The capability of FLQDs probe to escape from the reticuloendothelial system (RES) was investigated by evaluating its blood circulation half-time following intravenous administration to healthy female nude mice. Analyzing the blood samples taken from the administrated animals demonstrated a relatively long circulation half-time of 3.8 h (Figure 3a and b). This prolonged

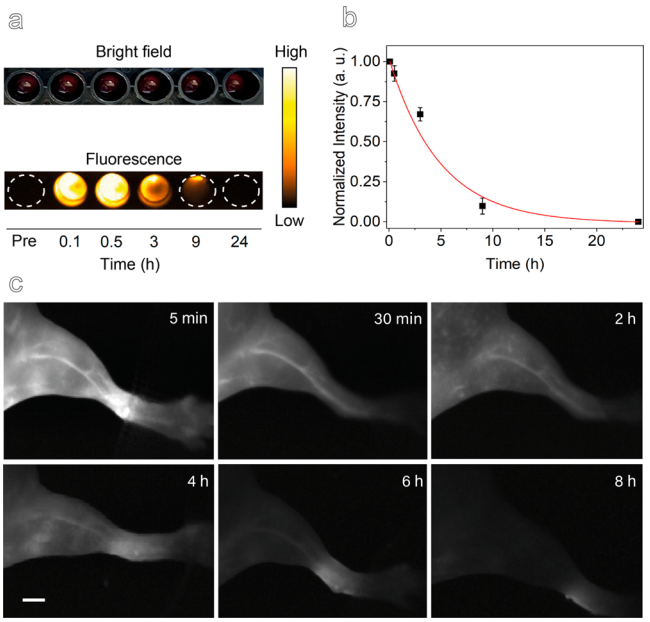

Figure 3. (a) Bright field and fluorescence images of the blood samples taken from a mouse treated by FLQDs probe. (b) Normalized fluorescence intensity plot and its corresponding fitting curve result in a mean half-time value of 3.8 h for blood circulation. The error bars represent the standard deviation (n = 3). (c) Hind limb vasculature fluorescence images of the mouse administered the probe, at different time points post injection. The scale bar represents 2.5 mm.

blood circulation half-time was further verified qualitatively by taking fluorescence images of mouse hind limb vasculature at specific time points after intravenous injection of the probe. As shown in Figure 3c, the vasculature could be easily detectable up to about 6 h post injection. Although the uptake rate by RES depends on many factors,[40] employing multi-arm PEG seems to provide longer blood longevity compared to the linear PEG-coated QDs. In particular, coating the prepared QD-MUA with linear PEG with characteristics similar to those employed in FLQDs led to a significantly lower blood circulation half-time (~50 min, Figure S8). It can be caused by the higher degree of steric hindrance provided by multiple arms of the multi-arm PEG ligands compared to linear ones. It is noteworthy that depending on the application of interest and the surface coating, the significantly high blood retention half-time of ~14 h could be achievable by Ag_2S QDs.[45]

Additionally, the *in vivo* blood vessel imaging performed shortly after the injection demonstrated that the probe could visualize the vascular networks of the animal, with the capability of discerning vessels as narrow as 36 μm in diameter (Figure 4). The result indicates that the fluorescent mode of the probes might be helpful in tracking angiogenesis mediated by tiny tumors.

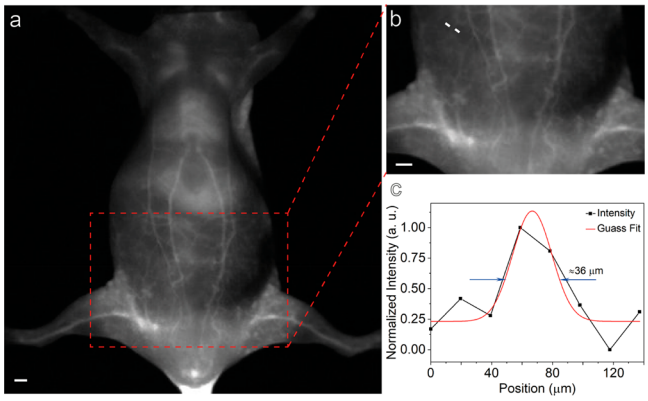

Figure 4. (a) *In vivo* fluorescence imaging of blood vessels. (b) Enlarged part of the image in frame(a). The dashed line indicates the narrowest vessel visualized by the probe. (c) The corresponding plot profile and its Gauss function fit, for the vessel shown in frame(b). The scale bar in frame(a) represents 2.5 mm and in frame(b) represents 3.2 mm.

Next, the *in vivo* propensity of the as-synthesized probes to target the induced tumor in living mice was evaluated. Following the intravenous injection of FLQDs and c-FLQDs probes into two separate groups of 4T1 tumor bearing mice, a series of fluorescence images were taken at specific time points. As seen from Figure S9, although the non-cRGD-conjugated probe could passively target the tumor through the EPR effect, the cRGD-conjugated one exhibited more efficient targeting ability, resulting in a higher signal-to-noise ratio (Figure S10). The higher tumor accumulation and lower nonspecific uptake of the cRGD-conjugated probe compared to its nonconjugated counterpart, was also confirmed by *ex vivo* studies assisted by fluorescence imaging and inductively coupled plasma mass spectrometry (ICP-MS) measurement (Figures S11 and S12).

Self-Illuminating Properties of the Probes. Intrigued by the great *in vitro* and *in vivo* performances of Ag_2S QDs confirmed by fluorescence mode, next we embarked upon evaluating the self-illuminating capability of the probe prepared through route 2. As one of the most essential prerequisites for effective BRET occurrence, the existence of a spectral overlap between the excitation profile of the acceptor and the emission of the donor was examined and the results are shown in Figure 5a. As seen from the figure, the excitation spectrum of the BLQDs can nicely cover the light arising from the NLuc-furimazine reaction (400–600 nm, λ_{peak} ~ 460 nm), suggesting that energy can be potentially transferred from donor to acceptor in the case where these two elements are in close

https://doi.org/10.1021/acsnano.2c06667
ACS Nano 2022, 16, 16824–16832

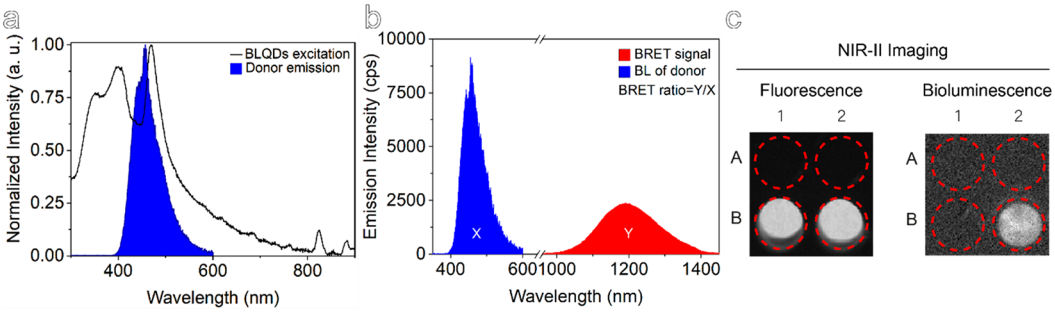

Figure 5. (a) Spectral overlap between the emission spectrum of the donor and the excitation spectrum of BLQDs. (b) Bioluminescence (BL) emission profile of NLuc and the NIR-II signal emitted following the occurrence of BRET between NLuc and BLQDs, subsequent to the addition of furimazine solution. The areas under the BL and BRET curves are denoted by X and Y, respectively. (c) NIR-II imaging of four wells of a 96-well plate filled with A1: water; A2: NLuc solution; B1: FLQDs; B2: BLQDs. The bioluminescence imaging was carried out immediately after the addition of furimazine solution to each well.

proximity and the QY of the acceptor is sufficiently high.[46] To verify, furimazine was added to two different solutions, namely, BLQDs and a mixture of FLQDs and NLuc solutions (ratio of QD to NLuc concentration was adjusted to be 1 to 10). Upon the addition and in the absence of any external excitation sources, the emission spectrum from the visible to NIR-II was collected. For the case of the former solution, two emission peaks at around 460 and 1200 nm were identified, attributed to the bioluminescence of furimazine and the BRET photons of QDs, respectively. These emission bands, displayed in Figure 5b, indicated the successful energy transfer between the donor−acceptor pair, certifying the self-illuminating capability of BLQDs probe. Through dividing the peak area of acceptor emission (1000−1400 nm) by that of donor (400−600 nm), an overall BRET ratio of 0.8 was obtained for the BLQDs probe. On the contrary, no NIR-II signal was captured from the latter solution containing FLQDs and unbounded NLuc, emphasizing the fact that in the process of BRET, the distance between the donor and acceptor is a matter of crucial importance (data are not shown). Moreover, to highlight the importance of the spectral overlap between the BRET constituents, firefly luciferase (FLuc) enzyme, which provides the highest QY among its counterparts,[47,48] was conjugated on the surface of QD-MUA in the exact manner mentioned for BL samples in route 2. Since the oxidation of D-luciferin, as the substrate of FLuc, gives rise to a red-shifted emission profile compared to NLuc (500−700 nm, $\lambda_{peak} \sim 560$ nm), a lower degree of spectral overlap was achieved (Figure S13). Consequently, employing the same experimental conditions did not lead to self-illuminating signals from the FLuc coated QDs (data are not shown). Although D-luciferin was already reported to successfully serve as the donor for a QD-based senor emitting in the visible region,[24] the much lower QY of NIR-II probes compared to that of their visible emitting counterparts[49] seems to limit the application of these red-shifted substrates as the internal excitation source for NIR-II emissive QDs.

To gain further insights into the efficiency of transferring energy between NLuc and Ag_2S QDs, Förster distance was calculated to determine the separation distance between these elements at which the efficiency is equal to 50% of its maximum value. The calculation led to an approximate number of 7.1 nm from which the curve of efficiency versus distance was obtained (Figure S14). On the other hand, the chain length of MUA ligands, which serve to immobilize NLuc on the surface of QDs in the designed decoration, has been reported to be 1.7 nm.[50] Moreover, the active pocket of NLuc which binds to furimazine to initiate the catalytic reaction was reported to be located in the center of the protein.[51] With all the aforementioned facts taken into consideration, the separation distance between the active pocket of the enzyme and the center of QD is expected to fall within the Förster distance, ensuring the efficient energy transfer between these two constituents of the designed BRET system.

Although employing BRET bestows the low background noise upon bioluminescence imaging, performing a proper background control is still recommended. In the absence of enzyme, the substrate might autonomously be oxidized, producing so-called "autoluminescence" light and leading to the background noise as well as erroneous readouts.[47] To investigate the potentiality of autoluminescence in initiating BRET, FLQDs and BLQDs along with water and NLuc solution were separately mixed with furimazine in different wells of a 96-well plate, followed by immediate bioluminescence and fluorescence imaging. The results illustrated in Figure 5c showed that although fluorescence signal can be detected from the wells containing QDs, bioluminescence light was only discernible from the case of BLQDs in which enzymes are anchored on the surface. Not only did the results show the capability of the NIR-II imaging system in detecting the BRET signal, but they also highlighted that autoluminescence, if existed, could not lead to detectable NIR-II photons. Furthermore, the efficacy of transferring energy in live 4T1 cells was assessed by incubating c-BLQDs with the cells in an Eppendorf tube. After the addition of the substrate to the tube, bioluminescence imaging was performed. The result illustrated in Figure 6a demonstrated that the NIR-II signal could be clearly visualized from the tube, confirming the *in vitro* self-illuminating capability of BLQDs, without inducing any toxicity.

Finally, the feasibility investigation of *in vivo* self-illuminating imaging by employing the biocompatible and NIR-II emissive Ag_2S QDs was examined. To this end, two groups of tumor bearing mice were treated with c-BLQDs probe. The first group, which received an intratumoral injection of a mixture of the probe and substrate, exhibited a bright bioluminescent signal (Figure 6b). Although the *in vivo* signal-to-noise ratio of bioluminescence imaging was ∼2 times that of fluorescence, ∼20 versus ∼10, the parameter rapidly (in about 1 min) dropped to lower the Rose criterion level, causing difficulties in employing the probe as a bioluminescence vessel imaging agent. While the glow-type characteristic of NLuc-furimazine

https://doi.org/10.1021/acsnano.2c06667
ACS Nano 2022, 16, 16824−16832

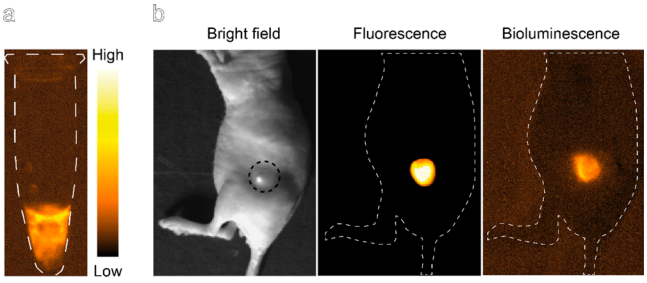

Figure 6. (a) *In vitro* NIR-II bioluminescence signal arising from live 4T1 cells incubated with c-BLQDs, following the addition of furimazine solution. (b) *In vivo* NIR-II fluorescence and bioluminescence imaging performed after injection of a mixture of c-BLQDs and substrate into the tumor site highlighted by black dashed circle.

reaction was previously reported to generate BRET signal with longer half-life in visible emitting QDs,[25] the quick decay of signal in our study which was observed for both the *in vitro* and *in vivo* cases (Figure S15a and b, respectively), might be attributed to the decreased QY of NIR-II QDs. It can be assumed that the catalytic reaction provides higher energy at the beginning of the reaction where there is a substantial amount of substrate available. As the reaction proceeds to consume the substrates, the energy might gradually decrease to a lower level which might not be sufficient to excite the QDs. Additionally, a suboptimal amount of BRET signal with a signal-to-noise ratio less than the Rose criterion was detected from the tumor site of each mouse in the second group, which were treated by intravenous injection of the probe followed by a 4 h delayed intravenous injection of the substrate. These results indicate that the self-illuminating mode of the probe needs further optimization to increase its BRET intensity, enabling it to engage in more practical applications.

Nevertheless, the feasibility of utilizing a nontoxic NIR-II emissive acceptor for bioluminescence imaging has been confirmed by our work. This probe and its optimized counterpart, which is currently under preparation by our group, are potentially capable of addressing the shortcomings of the previously reported BRET-QD nanosystems.

Apart from chemically engineering the constituents involving in self-illuminating imaging, the fast technological advancement in developing highly sensitive cameras, such as shortwave infrared (SWIR) InGaAs detectors, to detect the dimmest NIR signals have assisted the self-illuminating *in vivo* imaging field to expand during the past two decades.[52] It is expected that in the foreseeable future, further technological improvement would allow researchers to access to higher performance instruments which might enable them to explore farther aspects of bioluminescent imaging in the NIR-II region. It is also important to mention that although the current imaging technologies have limited the application of bioluminescent imaging to small animals, recent efforts have been made to step toward the translation of the technique to larger animals and potentially humans.[53]

CONCLUSION

In this study, extending the visible light of NLuc to the NIR-II region utilizing a single BRET step and a nontoxic QD-based acceptor (Ag_2S) was successfully carried out. The resulting self-illuminating probe was subjected to various characterizations to confirm its favorable properties as a prospective *in vivo* bioluminescent agent. The results suggested that the designed probe could potentially overcome the shortcomings of its previously reported counterparts, in terms of biosafety and providing deeper bioluminescent imaging. Employing the latest generation of SWIR InGaAs camera, bright NIR-II bioluminescent signals were easily detectable from the tumor site of mice injected with a mixture of probe and its substrate, leading to ∼2 times higher signal-to-noise ratio compared to the signals captured under fluorescence mode. We believe that the establishment of a single-step BRET mechanism to generate the NIR-II bioluminescent signal offers a straightforward and attractive prospect in deep tissue bioluminescence imaging which might be promising for future studies utilizing other safe materials as the acceptor, enriching the choices of BRET probes for versatile biomedical studies. However, further efforts are needed to be focused on improving the BRET ratio of the nanosystem to ensure that the probe is capable of taking part in more complex bioimaging practices. Thus, our future study would be devoted to manipulating the system constituents, as such an enhanced bioluminescence signal can be achievable.

EXPERIMENTAL SECTION

Materials. All chemicals and reagents purchased were of analytical grade and used without further purification, unless otherwise stated. Sodium diethyldithiocarbamate ($((C_2H_5)_2NCS_2Na)$) was purchased from Adamas-Beta. Silver nitrate ($AgNO_3$) and acetone were obtained from Shanghai Lingfeng Chemical Reagent. 1-Dodecanethiol (DT), 11-mercaptoundecanoic acid (MUA), tetramethylammonium hydroxide pentahydrate (TMAH), *N*-hydroxysuccinimide (NHS), and 4-(*N*-maleimidomethyl)cyclohexane-1-carboxylic acid 3-sulfo-*N*-hydroxysuccinimide ester sodium salt (SulfoSMCC) were bought from Shanghai Aladdin Bio-Chem Technology. Chloroform was purchased from Thermo Scientific Chemicals. 1-(3-(Dimethylamino)propyl)-3-ethylcarbodiimide hydrochloride (EDC) was obtained from Shanghai Energy Chemical. Amine-functionalized six-armed PEG (MW:10 k) was supplied from Shanghai Ponsure Biological Technology. Bradford protein kit was provided by Sangon Biotech. Arginine-glycine-aspartic-(D-phenylalanine)-cysteine(amide cyclic(end)) (cRGD-SH) was synthesized by GL Biochem. Fetal bovine serum (FBS) was supplied by Thermo Fisher Scientific. Ethidium bromide (EB) and Tris-acetate-EDTA (TAE, 50×) buffer were obtained from Beyotime Biotechnology. RNA (2×) loading dye was purchased from Beijing Solarbio Science & Technology. Agarose powder was acquired from Vivantis Technologies. NanoLuc luciferase (NLuc) and its substrate (furimazine) were purchased from Promega. Roswell Park Memorial Institute (RPMI) 1640 medium and Dulbecco's modified eagle medium (DMEM) were purchased from Basal Media. Cell counting kit-8 (CCK-8) was purchased from APExBIO. Ultrafiltration tubes (30 kDa MW cutoff) were bought from Merck Millipore. 4−6-week-old female nude mice (14−16 g) were purchased from Chang Zhou Cavensla Experimental Animal Technology. The mice were treated in accordance with guidelines approved by the ethics committee of Soochow University with the approval number of 202104A0107.

Characterizations. FEI Tecnai G20 transmission electron microscope operating at an acceleration voltage of 200 kV was used to capture the TEM images. Absorption spectra were recorded on a PerkinElmer Lambda 35 UV/Vis spectrometer. The fluorescence emission and excitation profiles of samples were obtained on an Edinburgh FLS980 spectrofluorometer. In the case of BRET ratio determination, the excitation source was turned off and the spectra were collected immediately after the addition of furimazine solution (2% v/v). Dynamic light scattering (DLS) and particle surface charge analysis measurements were carried out on Malvern Zetasizer Nano ZS90 at 25 °C.

NIR-II Fluorescence and Bioluminescence Imaging. Suzhou NIR-Optics and NIRvana LN (for conducting experiments related to

https://doi.org/10.1021/acsnano.2c06667
ACS Nano 2022, 16, 16824−16832

self-illuminating properties) instruments were utilized to perform NIR-II *in vitro* and *in vivo* imaging. Long pass filters of 1000 and 950 nm were used for the instruments, respectively. The power density of 120 m/Wcm^2 was adjusted in the case of fluorescence imaging, using a 808 nm laser. For bioluminescence imaging, the signal was acquired immediately after the addition (or injection) of the substrate solution (2% v/v), while the excitation source was off. The acquisition times of 100 ms and 10 s were adjusted for fluorescence and bioluminescence imaging, respectively.

Gel Electrophoresis. TAE was diluted 50 times and used as the running buffer. To prepare the gel, 0.5 g of agarose powder was dissolved in 50 mL of the running buffer and was subjected to heating at 120 °C, until a homogeneous and transparent solution was achieved. At this stage, 5 μL of EB was added to the mixture and the solution was poured into an appropriate mold. To prepare the samples, a certain amount of the sample of interest was diluted using the RNA (2×) loading dye. A running voltage of 100 V was applied on the gel, for about 20 min. The gel was subjected to NIR-II fluorescence imaging to visualize the mobility of the samples inside the matrix.

Cell Incubation. 4T1 cells were cultured in RPMI 1640 medium supplemented with 10% (v/v) FBS and 1% (v/v) penicillin/streptomycin antibiotics. The cells were incubated at 37 °C under an atmosphere containing 5% CO_2 and 95% humidified air. The medium was changed every other day.

Cytotoxicity Experiment. Cells were seeded in 96-well plates (3×10^5 cells in 100 μL per well) and allowed to grow for about 24 h. The medium was removed, and the cells were incubated with different concentrations of FLQDs and c-FLQDs (0, 6.25, 12.5, 25, 50, and 100 μg/mL) for 48 h. The medium was changed and the cells were incubated with CCK-8 (0.5 mg/mL) for 1−1.5 h. The absorbance of CCK-8 at 450 nm was measured by using a microplate reader (Bio Tek, Synergy 2). Cell viability was expressed by the ratio of the absorbance values of the cells incubated with probe solution to those of the cells incubated with culture medium.

In Vitro Cell Targeting Ability. Cells were seeded in 6-well plates (5×10^3 cells in 1.5 mL per well) and allowed to grow for about 24 h. Following washing the wells with 1 × PBS, FLQDs and c-FLQDs probes were separately incubated with the cells, for different time intervals. Subsequent to lysis treatment, the silver concentration uptaken by the cells of each well was obtained by ICP-MS.

Blood Circulation Half-Time and Blood Vessel Imaging. Three healthy mice were intravenously injected with 200 μg of FLQDs probe. At specific time points post injection, 20 μL of blood sample was taken from the eye of each mouse. The fluorescence intensity of each sample was measured and served as an indication of QDs concentration at each specific time point. Moreover, 10 min post injection, fluorescence images of the animals in ventral position were taken. In addition, at specific time points, fluorescence images of the hind limb vasculature of the animals were obtained.

In Vivo and Ex Vivo Biodistribution Analyses. Two groups of tumor bearing mice (n = 3) were intravenously injected with 200 μg of FLQDs and c-FLQDs probes, respectively. Subsequently, a series of fluorescence images were acquired at specific time points post injection. The treated animals were sacrificed, and their major organs were collected and subjected to fluorescence imaging. The mean fluorescence intensity arising from each organ was determined and compared with its corresponding standard curve to calculate the approximate percent injected dose per gram. Moreover, the organs were dissolved in an appropriate lysis solution, and the concentrations of silver ions accumulated inside them were determined by ICP-MS.

in Vitro Energy Transferring Capability. A solution of c-BLQDs probe was incubated with 4T1 cells in an Eppendorf tube, for about 1 h on ice. Following washing the tube with 1 × PBS, the substrate was added to the tube and the bioluminescence imaging was immediately carried out.

in Vivo NIR-II Bioluminescence Imaging. Two groups (n = 3) of the tumor bearing mouse were treated by c-BLQDs probes. For the first group, 10−15 μg of the probe solution was mixed with the substrate solution and was directly injected inside the tumor. The bioluminescence signal was immediately captured by using NIRvana LN instrument. The second group of mice, however, was treated by intravenous injection of 200 μL of the probe solution with a concentration of 1 mg/mL. Subsequently, 4 h after the probe injection, substrate solution (2% v/v) was intravenously injected and the bioluminescence imaging was performed.

Data Analysis. The fluorescence and bioluminescence signal intensities were obtained by ImageJ software. The intensity arising from the tumor site (I_1), a neighboring site of tumor on the animal body (I_2) and a neighboring site of tumor outside of the body (I_3) contributed to measuring signal-to-noise ratio using $(I_1 - I_3)/(I_2 - I_3)$ equation. The integral calculation for Förster distance determination was carried out by Wolfram Mathematica.

ASSOCIATED CONTENT

Supporting Information

The Supporting Information is available free of charge at https://pubs.acs.org/doi/10.1021/acsnano.2c06667.

Detailed synthesis rout of the probes, basic characterizations, *in vivo* and *ex vivo* biodistribution experiments, Förster distance calculation and bioluminescence decay curves (PDF)

AUTHOR INFORMATION

Corresponding Author

Mingyuan Gao − *Key Laboratory of Radiation Medicine and Protection, School for Radiological and Interdisciplinary Sciences (RAD-X), Collaborative Innovation Center of Radiation Medicine of Jiangsu Higher Education Institutions, Soochow University, Suzhou 215123, P. R. China;* orcid.org/0000-0002-7360-3684; Email: gaomy@suda.edu.cn

Authors

Mohammad Javad Afshari − *Key Laboratory of Radiation Medicine and Protection, School for Radiological and Interdisciplinary Sciences (RAD-X), Collaborative Innovation Center of Radiation Medicine of Jiangsu Higher Education Institutions, Soochow University, Suzhou 215123, P. R. China;* orcid.org/0000-0001-5077-570X

Cang Li − *Key Laboratory of Radiation Medicine and Protection, School for Radiological and Interdisciplinary Sciences (RAD-X), Collaborative Innovation Center of Radiation Medicine of Jiangsu Higher Education Institutions, Soochow University, Suzhou 215123, P. R. China;* orcid.org/0000-0002-6828-6565

Jianfeng Zeng − *Key Laboratory of Radiation Medicine and Protection, School for Radiological and Interdisciplinary Sciences (RAD-X), Collaborative Innovation Center of Radiation Medicine of Jiangsu Higher Education Institutions, Soochow University, Suzhou 215123, P. R. China;* orcid.org/0000-0001-7654-8724

Jiabin Cui − *Key Laboratory of Radiation Medicine and Protection, School for Radiological and Interdisciplinary Sciences (RAD-X), Collaborative Innovation Center of Radiation Medicine of Jiangsu Higher Education Institutions, Soochow University, Suzhou 215123, P. R. China;* orcid.org/0000-0003-3047-9852

Shuwang Wu − *Key Laboratory of Radiation Medicine and Protection, School for Radiological and Interdisciplinary Sciences (RAD-X), Collaborative Innovation Center of Radiation Medicine of Jiangsu Higher Education Institutions, Soochow University, Suzhou 215123, P. R. China*

Complete contact information is available at:
https://pubs.acs.org/10.1021/acsnano.2c06667

Notes

The authors declare no competing financial interest.

ACKNOWLEDGMENTS

The authors are deeply grateful to professor Fan Zhang at Fudan University for his genuine collaboration with providing the access to Nirvana instrument to conduct bioluminescence imaging. We also are grateful to the financial support from the National Key Research and Development Program of China (2018YFA0208800), the National Natural Science Foundation of China (82130059, 82172003, 81720108024), and Priority Academic Program Development of Jiangsu Higher Education Institutions (PAPD).

REFERENCES

(1) Jing, L.; Yang, C.; Zhang, P.; Zeng, J.; Li, Z.; Gao, M. Nanoparticles Weaponized with Built-In Functions for Imaging-Guided Cancer Therapy. *VIEW* **2020**, *1*, 19−33.
(2) Lu, L.; Li, B.; Ding, S.; Fan, Y.; Wang, S.; Sun, C.; Zhao, M.; Zhao, C.-X.; Zhang, F. NIR-II Bioluminescence for In Vivo High Contrast Imaging and In Situ ATP-Mediated Metastases Tracing. *Nat. Commun.* **2020**, *11*, 4192−4203.
(3) Jaunich, M.; Raje, S.; Kim, K.; Mitra, K.; Guo, Z. Bio-Heat Transfer Analysis During Short Pulse Laser Irradiation of Tissues. *Int. J. Heat Mass Transfer* **2008**, *51*, 5511−5521.
(4) Zhan, Q.; Qian, J.; Liang, H.; Somesfalean, G.; Wang, D.; He, S.; Zhang, Z.; Andersson-Engels, S. Using 915 nm Laser Excited Tm^{3+}/Er^{3+}/Ho^{3+}-Doped Naybf4 Upconversion Nanoparticles for In Vitro and Deeper In Vivo Bioimaging without Overheating Irradiation. *ACS Nano* **2011**, *5*, 3744−3757.
(5) Diao, S.; Hong, G.; Antaris, A. L.; Blackburn, J. L.; Cheng, K.; Cheng, Z.; Dai, H. Biological Imaging without Autofluorescence in the Second Near-Infrared Region. *Nano Res.* **2015**, *8*, 3027−3034.
(6) Li, Q.; Zeng, J.; Miao, Q.; Gao, M. Self-Illuminating Agents for Deep-Tissue Optical Imaging. *Front. Bioeng. Biotechnol.* **2019**, *7*, 326−338.
(7) Yang, Y.; Wang, S.; Lu, L.; Zhang, Q.; Yu, P.; Fan, Y.; Zhang, F. NIR-II Chemiluminescence Molecular Sensor for In Vivo High-Contrast Inflammation Imaging. *Angew. Chem., Int. Ed.* **2020**, *59*, 18380−18385.
(8) Hall, M. P.; Unch, J.; Binkowski, B. F.; Valley, M. P.; Butler, B. L.; Wood, M. G.; Otto, P.; Zimmerman, K.; Vidugiris, G.; Machleidt, T.; Robers, M. B.; Benink, H. A.; Eggers, C. T.; Slater, M. R.; Meisenheimer, P. L.; Klaubert, D. H.; Fan, F.; Encell, L. P.; Wood, K. V. Engineered Luciferase Reporter from a Deep Sea Shrimp Utilizing a Novel Imidazopyrazinone Substrate. *ACS Chem. Biol.* **2012**, *7*, 1848−1857.
(9) Hong, G.; Antaris, A. L.; Dai, H. Near-Infrared Fluorophores for Biomedical Imaging. *Nat. Biomed. Eng.* **2017**, *1*, 10−32.
(10) Frangioni, J. V. In Vivo Near-Infrared Fluorescence Imaging. *Curr. Opin. Chem. Biol.* **2003**, *7*, 626−634.
(11) Jathoul, A. P.; Grounds, H.; Anderson, J. C.; Pule, M. A. A Dual-Color Far-Red to Near-Infrared Firefly Luciferin Analogue Designed for Multiparametric Bioluminescence Imaging. *Angew. Chem., Int. Ed.* **2014**, *53*, 13059−13063.
(12) Kam, N. W. S.; O'Connell, M.; Wisdom, J. A.; Dai, H. Carbon Nanotubes as Multifunctional Biological Transporters and Near-Infrared Agents for Selective Cancer Cell Destruction. *Proc. Natl. Acad. Sci. U. S. A.* **2005**, *102*, 11600−11605.
(13) So, M. K.; Xu, C.; Loening, A. M.; Gambhir, S. S.; Rao, J. Self-Illuminating Quantum Dot Conjugates for In Vivo Imaging. *Nat. Biotechnol.* **2006**, *24*, 339−343.
(14) Xia, Z.; Xing, Y.; So, M.-K.; Koh, A. L.; Sinclair, R.; Rao, J. Multiplex Detection of Protease Activity with Quantum Dot Nanosensors Prepared by Intein-Mediated Specific Bioconjugation. *Anal. Chem.* **2008**, *80*, 8649−8655.
(15) Yao, H.; Zhang, Y.; Xiao, F.; Xia, Z.; Rao, J. Quantum Dot/Bioluminescence Resonance Energy Transfer Based Highly Sensitive Detection of Proteases. *Angew. Chem., Int. Ed.* **2007**, *46*, 4346−4349.
(16) Cissell, K. A.; Campbell, S.; Deo, S. K. Rapid, Single-Step Nucleic Acid Detection. *Anal. Bioanal. Chem.* **2008**, *391*, 2577−2581.
(17) Kumar, M.; Zhang, D.; Broyles, D.; Deo, S. K. A Rapid, Sensitive, and Selective Bioluminescence Resonance Energy Transfer (BRET)-Based Nucleic Acid Sensing System. *Biosens. Bioelectron.* **2011**, *30*, 133−139.
(18) Quiñones, G. A.; Miller, S. C.; Bhattacharyya, S.; Sobek, D.; Stephan, J. P. Ultrasensitive Detection of Cellular Protein Interactions Using Bioluminescence Resonance Energy Transfer Quantum Dot-Based Nanoprobes. *J. Cell. Biochem.* **2012**, *113*, 2397−2405.
(19) Feugang, J. M.; Youngblood, R. C.; Greene, J. M.; Fahad, A. S.; Monroe, W. A.; Willard, S. T.; Ryan, P. L. Application of Quantum Dot Nanoparticles for Potential Non-Invasive Bio-Imaging of Mammalian Spermatozoa. *J. Nanobiotechnol.* **2012**, *10*, 45.
(20) Hsu, C. Y.; Chen, C. W.; Yu, H. P.; Lin, Y. F.; Lai, P. S. Bioluminescence Resonance Energy Transfer Using Luciferase-Immobilized Quantum Dots for Self-Illuminated Photodynamic Therapy. *Biomaterials* **2013**, *34*, 1204−1212.
(21) Xing, Y.; So, M. K.; Koh, A. L.; Sinclair, R.; Rao, J. Improved QD-BRET Conjugates for Detection and Imaging. *Biochem. Biophys. Res. Commun.* **2008**, *372*, 388−394.
(22) Steven, C. M.; Lucia, B.; Pete, Y.; Sukanta, B.; Daniel, S. Self-Illuminating Nanoprobe for In Vivo Imaging of Cancers Over-Expressing the Folate Receptor. *Proc. SPIE* **2012**, 8233−8236.
(23) Hasegawa, M.; Tsukasaki, Y.; Ohyanagi, T.; Jin, T. Bioluminescence Resonance Energy Transfer Coupled Near-Infrared Quantum Dots Using GST-Tagged Luciferase for In Vivo Imaging. *Chem. Commun.* **2013**, *49*, 228−230.
(24) Yuan, C.; Wang, L.; An, Y.; Wu, G.; Zhang, D. Luciferase Gene-Loaded CS-Qdots as Self-Illuminating Probes for Specific Hepatoma Imaging. *RSC Adv.* **2015**, *5*, 29048−29057.
(25) Kamkaew, A.; Sun, H.; England, C. G.; Cheng, L.; Liu, Z.; Cai, W. Quantum Dot-NanoLuc Bioluminescence Resonance Energy Transfer Enables Tumor Imaging and Lymph Node Mapping In Vivo. *Chem. Commun.* **2016**, *52*, 6997−7000.
(26) Tsuboi, S.; Jin, T. Recombinant Protein (Luciferase-IgG Binding Domain) Conjugated Quantum Dots for BRET-Coupled Near-Infrared Imaging of Epidermal Growth Factor Receptors. *Bioconjugate Chem.* **2018**, *29*, 1466−1474.
(27) Wu, Q.; Chu, M. Self-Illuminating Quantum Dots for Highly Sensitive In Vivo Real-Time Luminescent Mapping of Sentinel Lymph Nodes. *Int. J. Nanomed.* **2012**, *7*, 3433−3443.
(28) Xiong, L.; Shuhendler, A. J.; Rao, J. Self-luminescing BRET-FRET Near-Infrared Dots for In Vivo Lymph-Node Mapping and Tumour Imaging. *Nat. Commun.* **2012**, *3*, 1193−1193.
(29) Zhang, Y.; Hong, G.; Zhang, Y.; Chen, G.; Li, F.; Dai, H.; Wang, Q. Ag_2S Quantum Dot: a Bright and Biocompatible Fluorescent Nanoprobe in the Second Near-Infrared Window. *ACS Nano* **2012**, *6*, 3695−3702.
(30) Li, C.; Li, W.; Liu, H.; Zhang, Y.; Chen, G.; Li, Z.; Wang, Q. An Activatable NIR-II Nanoprobe for In Vivo Early Real-Time Diagnosis of Traumatic Brain Injury. *Angew. Chem., Int. Ed.* **2020**, *132*, 253−258.
(31) Hong, G.; Robinson, J. T.; Zhang, Y.; Diao, S.; Antaris, A. L.; Wang, Q.; Dai, H. In Vivo Fluorescence Imaging with Ag_2S Quantum Dots in the Second Near-Infrared Region. *Angew. Chem., Int. Ed.* **2012**, *51*, 9818−9821.
(32) Li, C.; Zhang, Y.; Wang, M.; Zhang, Y.; Chen, G.; Li, L.; Wu, D.; Wang, Q. In Vivo Real-Time Visualization of Tissue Blood Flow and Angiogenesis Using Ag_2S Quantum Dots in the NIR-II Window. *Biomaterials* **2014**, *35*, 393−400.
(33) Wu, C.; Zhang, Y.; Li, Z.; Li, C.; Wang, Q. A Novel Photoacoustic Nanoprobe of ICG@PEG-Ag_2S for Atherosclerosis Targeting and Imaging In Vivo. *Nanoscale* **2016**, *8*, 12531−12539.

(34) Li, C.; Cao, L.; Zhang, Y.; Yi, P.; Wang, M.; Tan, B.; Deng, Z.; Wu, D.; Wang, Q. Preoperative Detection and Intraoperative Visualization of Brain Tumors for More Precise Surgery: A New Dual-Modality MRI and NIR Nanoprobe. *Small* **2015**, *11*, 4517−4525.
(35) Li, C.; Li, F.; Zhang, Y.; Zhang, W.; Zhang, X.-E.; Wang, Q. Real-Time Monitoring Surface Chemistry-Dependent In Vivo Behaviors of Protein Nanocages via Encapsulating an NIR-II Ag_2S Quantum Dot. *ACS Nano* **2015**, *9*, 12255−12263.
(36) Chen, G.; Lin, S.; Huang, D.; Zhang, Y.; Li, C.; Wang, M.; Wang, Q. Revealing the Fate of Transplanted Stem Cells In Vivo with a Novel Optical Imaging Strategy. *Small* **2018**, *14*, 1702679−1702689.
(37) Chen, G.; Tian, F.; Zhang, Y.; Zhang, Y.; Li, C.; Wang, Q. Tracking of Transplanted Human Mesenchymal Stem Cells in Living Mice Using Near-Infrared Ag_2S Quantum Dots. *Adv. Funct. Mater.* **2014**, *24*, 2481−2488.
(38) Purushothaman, B.; Song, J. M. Ag_2S Quantum Dot Theragnostics. *Biomater. Sci.* **2021**, *9*, 51−69.
(39) Walker, J. R.; Hall, M. P.; Zimprich, C. A.; Robers, M. B.; Duellman, S. J.; Machleidt, T.; Rodriguez, J.; Zhou, W. Highly Potent Cell-Permeable and Impermeable NanoLuc Luciferase Inhibitors. *ACS Chem. Biol.* **2017**, *12*, 1028−1037.
(40) Blanco, E.; Shen, H.; Ferrari, M. Principles of Nanoparticle Design for Overcoming Biological Barriers to Drug Delivery. *Nat. biotechnol.* **2015**, *33*, 941−951.
(41) Havaki, S.; Kouloukoussa, M.; Amawi, K.; Drosos, Y.; Arvanitis, L. D.; Goutas, N.; Vlachodimitropoulos, D.; Vassilaros, S. D.; Katsantoni, E. Z.; Voloudakis-Baltatzis, I.; Aleporou-Marinou, V.; Kittas, C.; Marinos, E. Altered Expression Pattern of Integrin Alphavbeta3 Correlates with Actin Cytoskeleton in Primary Cultures of Human Breast Cancer. *Cancer Cell Int.* **2007**, *7*, 16−29.
(42) Dong, B.; Li, C.; Chen, G.; Zhang, Y.; Zhang, Y.; Deng, M.; Wang, Q. Facile Synthesis of Highly Photoluminescent Ag_2Se Quantum Dots as a New Fluorescent Probe in the Second Near-Infrared Window for In Vivo Imaging. *Chem. Mater.* **2013**, *25*, 2503−2509.
(43) Xie, R.; Rutherford, M.; Peng, X. Formation of High-Quality I-III-VI Semiconductor Nanocrystals by Tuning Relative Reactivity of Cationic Precursors. *J. Am. Chem. Soc.* **2009**, *131*, 5691−5697.
(44) Sriraman, S. K.; Aryasomayajula, B.; Torchilin, V. P. Barriers to Drug Delivery in Solid Tumors. *Tissue Barriers* **2014**, *2*, 29528−29530.
(45) Song, C.; Zhang, Y.; Li, C.; Chen, G.; Kang, X.; Wang, Q. Enhanced Nanodrug Delivery to Solid Tumors Based on a Tumor Vasculature-Targeted Strategy. *Adv. Funct. Mater.* **2016**, *26*, 4192−4200.
(46) Lakowicz, J. R. *Principles of fluorescence spectroscopy*; Springer: Baltimore, 2006; pp 1−26.
(47) Badr, C. E. Bioluminescence Imaging: Basics and Practical Limitations. *Methods Mol. Biol.* **2014**, *1098*, 1−18.
(48) Syed, A. J.; Anderson, J. C. Applications of Bioluminescence in Biotechnology and Beyond. *Chem. Soc. Rev.* **2021**, *50*, 5668−5705.
(49) Li, C.; Chen, G.; Zhang, Y.; Wu, F.; Wang, Q. Advanced Fluorescence Imaging Technology in the Near-Infrared-II Window for Biomedical Applications. *J. Am. Chem. Soc.* **2020**, *142*, 14789−14804.
(50) Hinterwirth, H.; Kappel, S.; Waitz, T.; Prohaska, T.; Lindner, W.; Lämmerhofer, M. Quantifying Thiol Ligand Density of Self-Assembled Monolayers on Gold Nanoparticles by Inductively Coupled Plasma-Mass Spectrometry. *ACS Nano* **2013**, *7*, 1129−1136.
(51) Tomabechi, Y.; Hosoya, T.; Ehara, H.; Sekine, S.-i.; Shirouzu, M.; Inouye, S. Crystal Structure of NanoKAZ: The Mutated 19 kDa Component of Oplophorus Luciferase Catalyzing the Bioluminescent Reaction with Coelenterazine. *Biochem. Biophys. Res. Commun.* **2016**, *470*, 88−93.
(52) Liu, S.; Su, Y.; Lin, M. Z.; Ronald, J. A. Brightening up Biology: Advances in Luciferase Systems for In Vivo Imaging. *ACS Chem. Biol.* **2021**, *16*, 2707−2718.
(53) Yevtodiyenko, A.; Bazhin, A.; Khodakivskyi, P.; Godinat, A.; Budin, G.; Maric, T.; Pietramaggiori, G.; Scherer, S. S.; Kunchulia, M.; Eppeldauer, G.; Polyakov, S. V.; Francis, K. P.; Bryan, J. N.; Goun, E. A. Portable Bioluminescent Platform for In Vivo Monitoring of Biological Processes in Non-Transgenic Animals. *Nat. Commun.* **2021**, *12*, 2680−2692.

https://doi.org/10.1021/acsnano.2c06667
ACS Nano 2022, 16, 16824−16832